Core barrier formation near integer *q* surfaces in DIII-D[a)]

M. E. Austin,[1,b)] K. H. Burrell,[2] R. E. Waltz,[2] K. W. Gentle,[1] P. Gohil,[2] C. M. Greenfield,[2] R. J. Groebner,[2] W. W. Heidbrink,[3] Y. Luo,[3] J. E. Kinsey,[4] M. A. Makowski,[5] G. R. McKee,[6] R. Nazikian,[7] C. C. Petty,[2] R. Prater,[2] T. L. Rhodes,[8] M. W. Shafer,[6] and M. A. Van Zeeland[9]

[1]*University of Texas at Austin, Austin, Texas 78712*
[2]*General Atomics, P.O. Box 85608, San Diego, California 92186-5608*
[3]*University of California at Irvine, Irvine, California 92612*
[4]*Lehigh University, Bethlehem, Pennsylvania 18015*
[5]*Lawrence Livermore National Laboratory, Livermore, California 94550*
[6]*University of Wisconsin at Madison, Madison, Wisconsin 53706*
[7]*Princeton Plasma Physics Laboratory, Princeton, New Jersey 08540*
[8]*University of California at Los Angeles, Los Angeles, California 90032*
[9]*Oak Ridge Institute for Science Education, Oak Ridge, Tennessee 37831-0117*

(Received 10 April 2006; accepted 10 July 2006; published online 4 August 2006)

Recent DIII-D experiments have significantly improved the understanding of internal transport barriers (ITBs) that are triggered close to the time when an integer value of the minimum in q is crossed. While this phenomenon has been observed on many tokamaks, the extensive transport and fluctuation diagnostics on DIII-D have permitted a detailed study of the generation mechanisms of q-triggered ITBs as pertaining to turbulence suppression dynamics, shear flows, and energetic particle modes. In these discharges, the evolution of the q profile is measured using motional Stark effect polarimetry and the integer $q_{\min}$ crossings are further pinpointed in time by the observation of Alfvén cascades. High time resolution measurements of the ion and electron temperatures and the toroidal rotation show that the start of improved confinement is simultaneous in all three channels, and that this event precedes the traversal of integer $q_{\min}$ by 5–20 ms. There is no significant low-frequency magnetohydrodynamic activity prior to or just after the crossing of the integer $q_{\min}$ and hence magnetic reconnection is determined not to be the precipitant of the confinement change. Instead, results from the GYRO code point to the effects of zonal flows near low order rational q values as playing a role in ITB triggering. A reduction in local turbulent fluctuations is observed at the start of the temperature rise and, concurrently, an increase in turbulence poloidal flow velocity and flow shear is measured with the beam emission spectroscopy diagnostic. For the case of a transition to an enduring internal barrier the fluctuation level remains at a reduced amplitude. The timing and nature of the temperature, rotation, and fluctuation changes leading to internal barriers suggests transport improvement due to increased shear flow arising from the zonal flow structures. © *2006 American Institute of Physics*. [DOI: 10.1063/1.2245579]

I. INTRODUCTION

Central to the goal of obtaining high performance fusion discharges in tokamaks is understanding how transitions to improved confinement occur. In particular, understanding the mechanisms of internal transport barrier (ITB) formation is critical since this may provide a means of running a tokamak fusion reactor at enhanced parameters, thus allowing a reduction in size.

In DIII-D (Refs. 1 and 2) as well as JT-60U,[3] RTP,[4] TFTR,[5] JET,[6] ASDEX-U,[7] and T10,[8] it has been observed that the formation and performance of ITB discharges is linked to surfaces where the safety factor q has low-order rational values, particularly integer surfaces. In experiments in these devices, transport improvement either was initiated at and/or transport barriers were tied to locations with q =integer. In many cases the integer q was located at the minimum in the q profile in a negative central shear discharge, with the surface roughly half way out in the plasma minor radius.

Theories proposed to explain transitions to improved confinement at rational q fall into two categories. The first postulates that the occurrence of magnetohydrodynamic (MHD) instabilities, such as tearing modes or fishbones, causes changes in E_r and hence the $E\times B$ flow shear leading to reduction of microinstability-induced transport.[6,7] The second relies on the existence of intrinsically good magnetic surfaces having highly irrational q values which are in close proximity to low-order rational surfaces. This is essentially the basis for models invoking rarefaction of rational surfaces,[9] noble cantor sets,[10] and paleoclassical transport.[11] Experimentally distinguishing between the two cases would at first glance seem to be easy; since with evolving q profiles the gap in rational surfaces is encountered before the rational

[a)]This paper is based on an invited paper presented at the annual APS DPP Meeting in Denver, Colorado, October 2005. Paper CI1b 4, Bull. Am. Phys. Soc. **50**, 64 (2005).
[b)]Invited speaker.

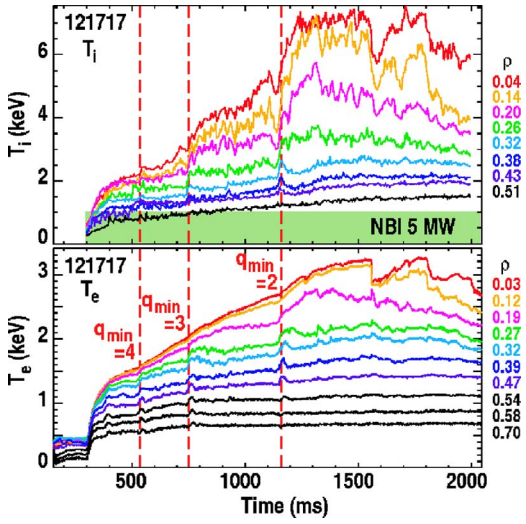

FIG. 1. Ion and electron temperature time traces for a typical NCS ITB shot (I_p=1.2 MA, B_T=2.0 T). The $q_{\min}$=integer times are determined from MSE-constrained EFIT reconstructions and RSAE modes. The ITB is triggered at 1150 ms with 5 MW of NB power. The drop in central temperatures at 1550 ms is caused by the onset of a core MHD mode.

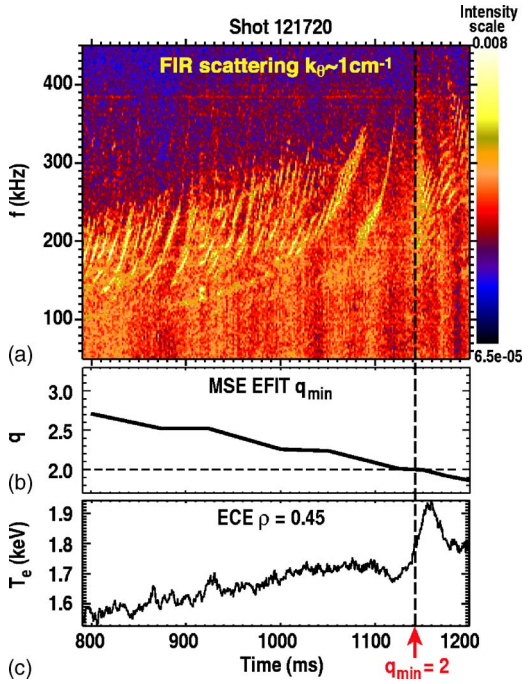

FIG. 2. (a) Spectrogram of FIR scattering low-k (k_θ~0–1 cm^{-1}) data showing RSAE modes and the burst that begins at $q_{\min}$=2 for discharge 121720. (b) $q_{\min}(t)$ derived from MSE EFITs. (c) T_e from ECE near the $q_{\min}$ radius.

surface itself, barrier formation occurring before $q=m/n$ is reached and without MHD activity would seem to point to the second category. However, the time window between irrational and rational surfaces can be short, ~5–10 ms, within the experimental uncertainty of some barrier-indicating diagnostics. In addition, certain types of MHD modes in the core can be difficult to detect, especially high frequency, beam ion driven instabilities such as Alfvén eigenmodes. In order to gain further insight into the nature of ITB triggering at rational values of the minimum in $q(q_{\min})$ it is apparent that high quality, high temporal and spatial resolution measurements of transport quantities (e.g., electron temperature T_e, ion temperature T_i, and radial electric field E_r) and MHD activity are required.

In this paper a class of discharges in the DIII-D tokamak where changes to transport are clearly triggered as an integer $q_{\min}$ is traversed are studied in detail with a broad set of diagnostics. The time period of the transition is examined closely for the timing of changes to temperature, rotation, turbulence, and MHD modes.

II. TIMING AND BEHAVIOR OF TRANSPORT CHANGES NEAR $q_{\min}$=2

The types of DIII-D pulses exhibiting clear transport changes at low-order rational values of $q_{\min}$ are low density, L-mode discharges with early neutral beam (NB) injection yielding negative central shear (NCS) in the core. A typical example of the temperature behavior is shown in Fig. 1. These discharges with constant NB heating power show spontaneous increases in T_i, T_e, and toroidal rotation v_ϕ as the current profile evolves and the $q_{\min}$=4,3,2 surfaces come into the plasma. Typically, the crossing of the q=2 surfaces initiates an ITB in the ions that can be seen in Fig. 1 from the increase in separation of the traces for $0.15<\rho<0.30$ indicating steep gradients there. It is important to note that these discharges at low heating power are marginal for transport barrier formation. At higher power transport barriers form independent of integer q values. Also, it is worth noting that the observed changes are in energy and momentum confinement, not particle confinement, i.e., there are no barriers observed in the density profiles.

The discharges discussed here are generally moderate beta plasmas, at least in the early phase β_N~0.7, where β_N is the normalized beta, $\beta_N=\%\beta/(I/aB_\phi)$. Hence MHD modes do not usually arise to affect transport. In the later stage, after the ITB forms, β_N increases typically to ≥1.0 and then MHD activity will often develop. This can be seen in Fig. 1 where at 1550 ms a core tearing mode starts and spoils confinement.

The q profiles in these discharges are measured with the motional Stark effect (MSE) diagnostic[12] and the time of integer $q_{\min}$ is pinpointed with the observation of Alfvén cascades, more properly referred to as Reverse Shear Alfvén Eigenmodes (RSAE). At integer values of $q_{\min}$, one expects a "grand cascade" of RSAEs, where all toroidal mode numbers n appear simultaneously thus marking in time this special value of q at the zero shear point.[13,14] These high frequency coherent modes are seen in the Fourier analyzed data from the far infrared (FIR) scattering diagnostic,[15] which measures density fluctuations at k_θ~1 cm^{-1}±1 cm^{-1}. Figure 2 displays an example of the RSAE modes indicating the time of $q_{\min}$=2 compared with MSE q measurements and the T_e changes that occur in this interval. Using the RSAE modes it is possible to determine the advent of the integer $q_{\min}$ surface to within 1–2 ms.

The timing of the temperature changes that mark the beginning of the improved transport phase and the crossing of the rational surface is of keen interest. As can be seen in

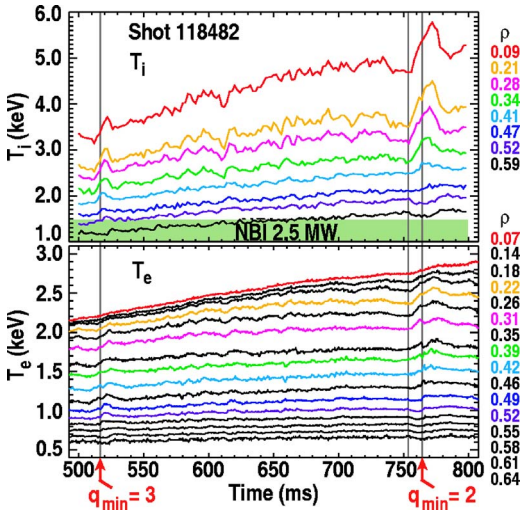

FIG. 3. Ion and electron temperature evolution for a NCS L-mode discharge heated with one NB source showing transient changes to transport at integer q_{min} times.

Fig. 3, the electron and ion temperature inside of $\rho=0.45$ starts to rise before $q_{min}=2$ is reached. This is a general result. The discharge of Fig. 3 is a NCS discharge heated with one NB source (2.5 MW) that has a transient phase of reduced transport near the time that the minimum in q traverses 2. From the RSAE modes, q_{min} crosses 2 at 764 ms, but the temperature rise in both T_i and T_e begins at 753 ms. (The time resolution of the T_i and T_e measurements is 1 ms and 0.5 ms respectively.) Close inspection of the temperature traces reveals that this is a true transport barrier in the sense that the channels outside of $\rho=0.5$ show a drop in temperature while the inner channels are rising. This observation is highlighted in Fig. 4 which displays for the shot of Fig. 3 the change in T_e profiles at several times around the $q_{min}=2$ time. There is a clear pivot radius, situated near the q_{min} radius, around which the δT_e profile either increases or decreases. This result is common for NCS shots with a single NB source; for shots heated with 5 MW of neutral beams, the temperature drop outside of the q_{min} radius is not always clearly observed perhaps because of the higher heat flux in these cases. In either case, the rise in T_e near the q_{min} radius is seen to start at 5–20 ms before $q_{min}=2$ comes into the plasma.

The fact that the temperature rise associated with the improved transport begins before q_{min} gets to 2 is strong evidence that reconnection and island formation is not required to initiate barrier formation. In addition, as shown in Fig. 5, no low frequency modes are detected in the magnetic probe data around the $q_{min}=2$ time in this class of discharges. It has been suggested in Refs. 7 and 16 that low m/n tearing modes could induce changes in E_r and thereby trigger transport changes. The DIII-D experiments indicate that this is not a necessary condition for barrier triggering.

The transient nature of the changes to electron transport in these shots can best be seen by looking at the time evolution of the T_e gradients in the vicinity of the q_{min} radius. Experimentally, $\nabla T_e(t)$ is obtained from the difference between pairs of adjacent electron cyclotron emission (ECE) channels divided by the radial separation of the channel resonance locations. Figure 6 is a plot of the time history of T_e gradients derived this way for three locations at and just

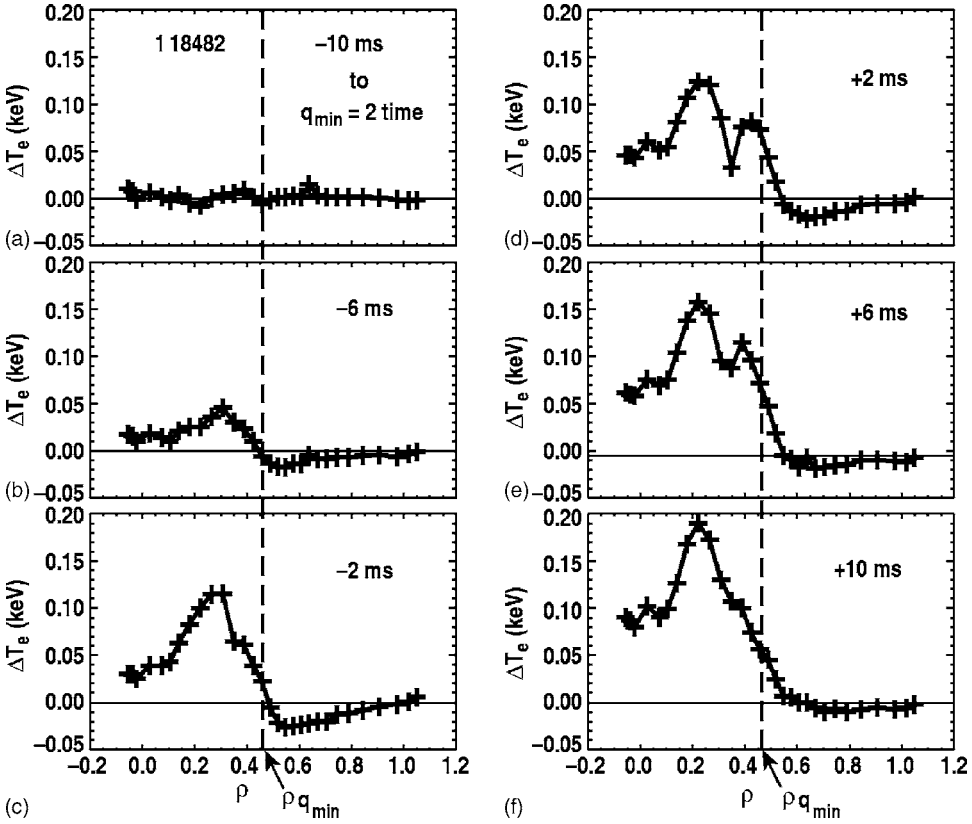

FIG. 4. δT_e profiles every 4 ms near the $q_{min}=2$ time for the shot of Fig. 3. Plots (a)–(c) are before the $q_{min}=2$ time, (d)–(f) are after. The δT_e profiles are referenced to 750 ms, 14 ms before the $q_{min}=2$ time.

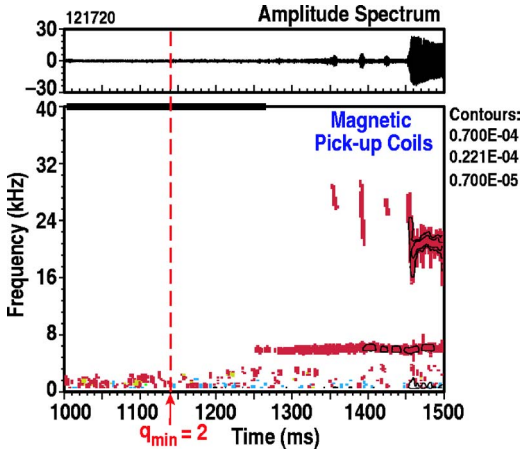

FIG. 5. A typical spectrogram of magnetic pick-up coil data for a NCS L-mode shot with an ITB triggered when $q_{\min}$ crosses 2, for this shot, at 1140 ms.

inside the $q_{\min}$ radius around the time of $q_{\min}=2$ for shot 118482 which had a transient improvement in confinement. The uncertainty in ∇T_e is chiefly due to the random temperature fluctuations and is calculated to be 0.2 in units of a/LTe. Figure 7 contains the same type of plots as Fig. 6 for shot 121717, a discharge with 5 MW of NB heating and which forms an internal transport barrier near the $q_{\min}=2$ time. Both figures show similar behavior around integer $q_{\min}$: a steepening prior to the $q_{\min}=2$ time, then a drop as $q=2$ is crossed, followed quickly by a resteepening and then a return to the initial gradient level or higher.

The experimentally observed T_e gradient behavior is similar to that found by the global gyrokinetic code GYRO.[17] As reported in Ref. 18, with smooth equilibrium input profiles, profiles produced in GYRO simulations of turbulence-

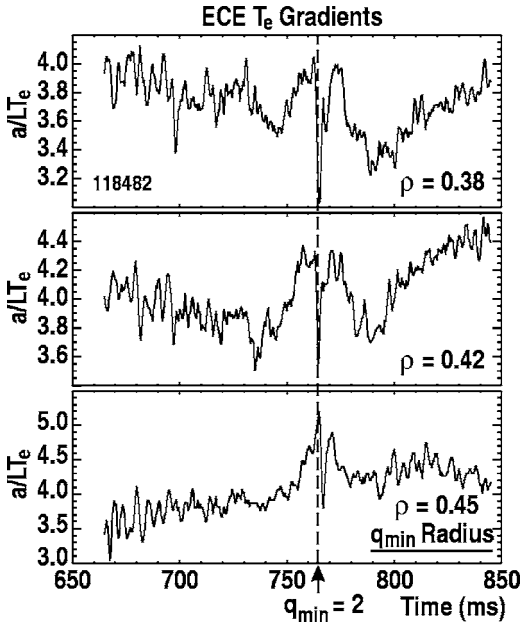

FIG. 6. $\nabla T_e(t)$ around the time $q_{\min}=2$ for three locations near the $q_{\min}$ radius for the shot of Fig. 3. The gradient amplitude is given in terms of a/L_{Te}, and the minor radius of the plasma divided by the electron temperature gradient scale length.

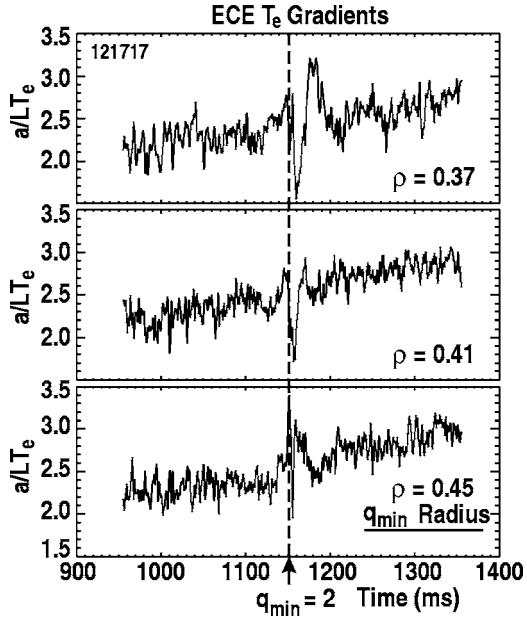

FIG. 7. $\nabla T_e(t)$ around the $q_{\min}=2$ time for three locations near the $q_{\min}$ radius for the two NB source shot of Fig. 1.

driven transport have large corrugations in the $T_e(r)$, $T_i(r)$, $n_e(r)$, and the electrostatic potential $\Phi(r)$ profiles at low order rational surfaces. These corrugations are the result of turbulent transport changes produced by zonal flows, which are toroidally and poloidally symmetric $\Phi(r)$ structures driven by the turbulence.[19] The previous results were obtained with monotonic q profiles; however, nonlinear GYRO simulations have recently been performed for a discharge with a reverse shear q profile and the results are shown in Fig. 8 for a case with $q_{\min}$ just below 2 at 1.98. This plot illustrates the typical features of the profile corrugations with the gradient sharply decreasing at the rational surface and increasing on either side. The GYRO run is for a plasma with equilibrium profiles constant in time; however, it is clear that for a plasma evolving on a time scale slower than a characteristic turbulence time, the gradient behavior for a fixed location near the minimum in q should be like that shown in Figs. 6 and 7, with the gradient increasing at intervals just before and after $q_{\min}=2$, and decreasing right at the $q_{\min}=2$ time. In light of the GYRO results, the T_e gradient data may be interpreted as the measurement of the temperature component of a zonal flow. An extensive discussion of these minimum-q profile simulations and a theory of the profile corrugations is given in Ref. 20.

The GYRO results predict that the profile corrugations should follow the $q=2$ surface as it splits and moves through the plasma. Indeed, as shown in Fig. 9, a dip and a bump in the T_e gradient moves inward to smaller radius and a bump moves outward to larger radius, both roughly following the $q=2$ surface as determined from MSE q profiles. These results match similar ones from JET shown in Ref. 6. The bump in ∇T_e moving inward is more prominent than the outward propagating one, perhaps because the region inside of $q_{\min}$ has negative magnetic shear, favorable for ITG mode

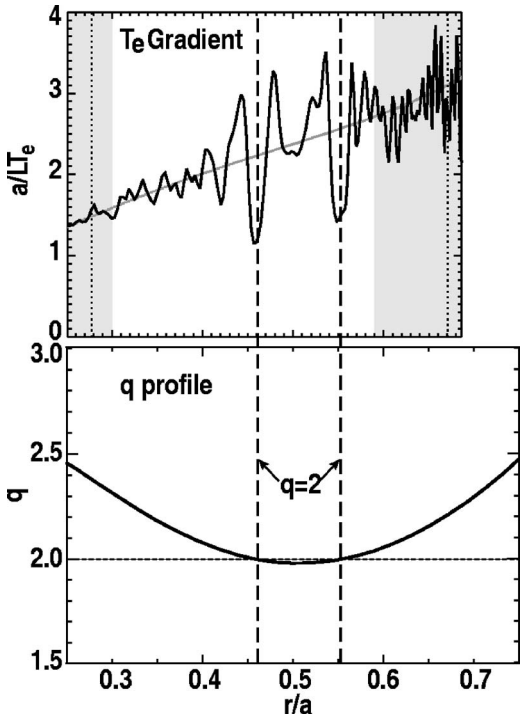

FIG. 8. T_e gradient versus normalized radius from a GYRO code simulation using the plasma conditions from shot 121717 at 1155 ms and the q profile for this time slice. The profile corrugations associated with the $q=2$ surfaces can be seen. The shaded region of the T_e gradient plot indicates the radii where the GYRO code resolution becomes poor.

suppression, whereas the outside region has positive magnetic shear, more favorable for ITG mode growth.

One area that is not clear in q-related transport changes is the role of the RSAE modes. Recent work has suggested these modes may interact with thermal ions.[21] In the discharges discussed here, a drop in core ion temperature is observed, just before the temperature rises associated with $q=3$ and $q=2$ as seen in Fig. 1 at 700 and 1100 ms, respectively. This core temperature loss, along with a drop in v_ϕ, is correlated with the onset of TAE modes that come after the

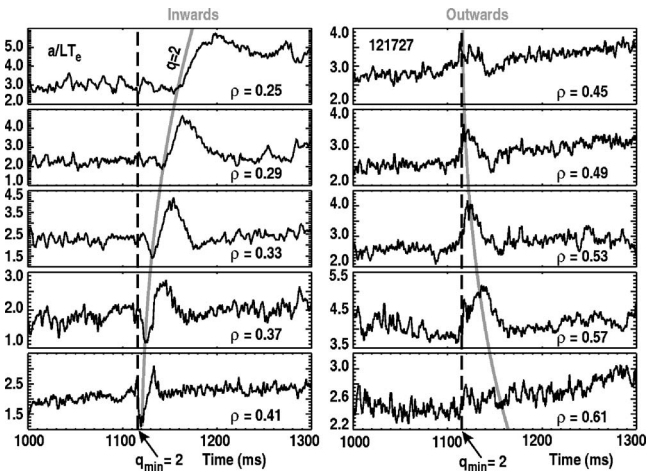

FIG. 9. $\nabla T_e(t)$ around the time $q_{\min}=2$ for ten radial positions in a discharge with ITB formation at the $q_{\min}=2$ time. The structure in the T_e gradient can be seen to propagate radially inwards and outwards.

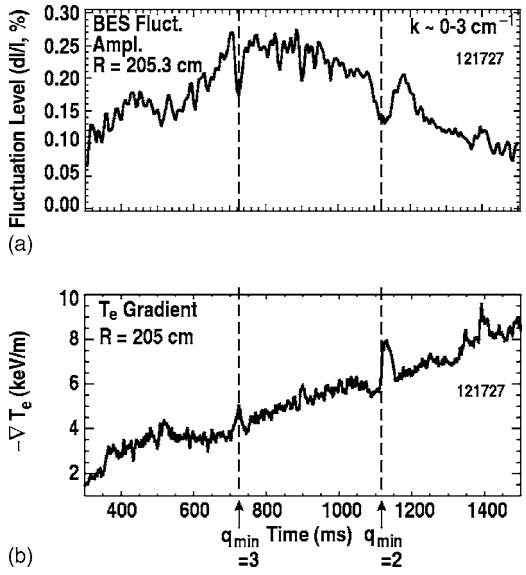

FIG. 10. (a) Fluctuation amplitude ($\tilde{n}_e/n_e$) versus time from the BES diagnostic for a shot with confinement improvement at the time of $q_{\min}=3$ and $q_{\min}=2$ crossings. (b) Local T_e gradient versus time at the BES measurement radius. The radius of the $q_{\min}$ is between 200 and 205 cm for this time window.

RSAE frequency chirp. The TAE modes are seen clearly in localized density fluctuation measurements by the beam emission spectroscopy (BES) diagnostic, and somewhat less clearly in edge magnetic probe data. However, fast ion spectroscopy measurements[22] indicate little or no fast ion loss at this time; also, there is no coincidental drop in neutron rate. These observations rule out fast ion losses that would lead to changes in E_r and hence effect transport via $E\times B$ shear changes. In the DIII-D experiments, a few shots were heated with beams that inject more perpendicularly to the magnetic axis and create a fast ion distribution less likely to drive energetic particle modes. In these shots, in which it is not possible to obtain CER or BES measurements, no TAE modes were seen in the magnetic probe data. The ECE T_e measurements show the identical transient transport improvements near integer $q_{\min}$ as shots with TAE modes, for example those in shown Figs. 1 and 7. This demonstrates that the RSAE modes are not actively contributing to the rational-q transport changes, but rather are just passively present.

III. CHANGES IN TURBULENT FLUCTUATIONS AND TRANSPORT NEAR $q_{\min}$=INTEGER

In the previous section we saw that transient changes in electron and ion transport appeared near low-order rational values of $q_{\min}$ and that the changes were connected to zonal flow structures. For the case of ion barrier formation, the transient events at the time where $q_{\min}=2$ seem to be the trigger for sustained improved core confinement. The question arises, what happens to the turbulent fluctuations during these periods?

Figure 10 shows a localized measurement of low-k ($k_\theta \sim 0$–3 cm^{-1}) density fluctuations from the BES diagnostic[23] for a shot with transient jumps in electron confinement near the times where $q_{\min}=3$ and $q_{\min}=2$. The mea-

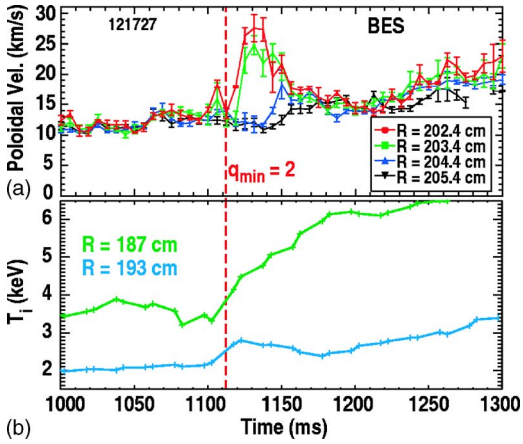

FIG. 11. (a) Poloidal velocity evolution derived from BES measurements near the $q_{\min}=2$ time for the same discharge as Fig. 10. (b) Core T_i versus time for two locations showing barrier formation at the $q_{\min}=2$ crossing.

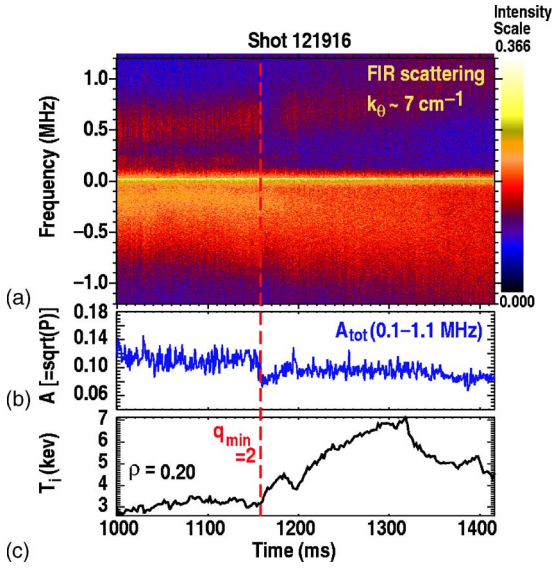

FIG. 12. (a) FIR scattering spectrogram for intermediate k_θ for a discharge with an ITB triggered at the $q_{\min}=2$ time. (b) Integrated amplitude for frequency band 0.1–1.1 MHz showing a drop in integrated fluctuation amplitude at the $q_{\min}=2$ time. (c) Core ion temperature channel showing the start of ITB at $q_{\min}=2$.

surement is made near the $q_{\min}$ radius, which is about 204 cm for this discharge. The data indicate a clear reduction in fluctuation amplitude at the integer $q_{\min}$ times that matches in time the local increase in T_e gradient that is the indication of improved transport. The transient dips in turbulent fluctuations are seen for BES positions 4 cm inward and outward from this position, but not for positions farther out in the minor radius. Measurements are not available for positions at smaller minor radius, but the largest transient drop in amplitude is for the position nearest $q_{\min}$; hence, it appears the reduction in turbulence is localized to the $q_{\min}$ radius.

The BES diagnostic is also capable of measuring the poloidal velocity of the turbulent eddies as discussed in Ref. 24. Figure 11 presents the results of this analysis for locations near the $q_{\min}$ radius around the time of $q_{\min}=2$ for a discharge with a transition to a core ion barrier. The data show a highly localized jump in poloidal velocity at this event. There is a question in these data about the effect of the RSAE modes, which also show up in the BES spectrograms, on the poloidal velocity determination. However, multiple analysis runs using different integration windows that exclude the cascade range of frequencies show very similar rotation changes, albeit with larger levels of noise. Accordingly, we are fairly confident that this is a valid measurement of the poloidal rotation. Taken at face value, the rotation measurements give a velocity shear of $1\times10^6\ s^{-1}$, a very large value and certainly a value sufficient to induce sustained improved confinement through shear suppression of turbulence. And it should be noted that the poloidal velocity increase starts before the time of $q_{\min}=2$ in similar fashion to the electron and ion changes preceding the integer $q_{\min}$ crossing, in accordance with the profile corrugations picture.

Changes to turbulent fluctuation levels near rational $q_{\min}$ have also been observed in the intermediate k range in these discharges. Figure 12 shows a spectrogram and a density fluctuation amplitude time history from the FIR scattering intermediate-k diagnostic ($k_\theta \sim 7\ cm^{-1}$). These data show a large drop in fluctuation amplitude at the $q_{\min}=2$ time and that the fluctuations remain at a reduced level subsequently, during the ITB phase. The FIR scattering integrates over a broad spatial range; the Doppler shift of these fluctuations suggest they are in the core of the discharge. The behavior is consistent with the picture of the reduced ion transport being due to $E\times B$ shear suppression of turbulence.[25,26]

Figure 13 displays the results from a TRANSP power balance analysis for one of these shots with an ITB triggered at $q_{\min}=2$, showing χ_i and χ_e versus time for three radii in the core. Near the time of $q_{\min}=2$ the core χ_i's drop sharply by roughly a factor of 2, confirming the core barrier formation. The χ_e's however show only a gradual reduction throughout the discharge, with a time behavior reflecting the current profile soak-in. (Note that short time scale changes to

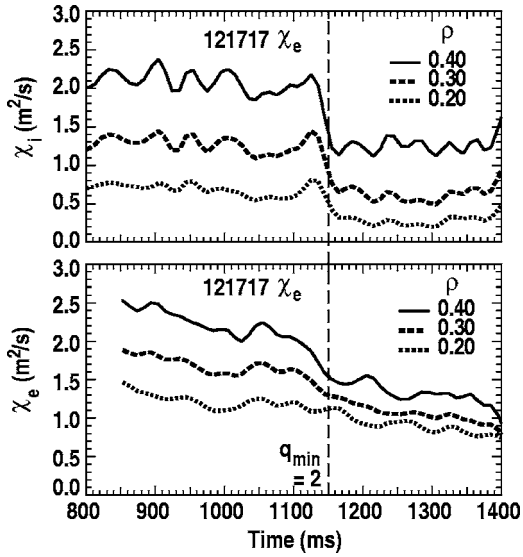

FIG. 13. Core ion and electron diffusivities versus time from TRANSP for the discharge of Fig. 1 showing the stepwise change in confinement in the ion channel at the $q_{\min}=2$ time, but no similar step in the electron channel.

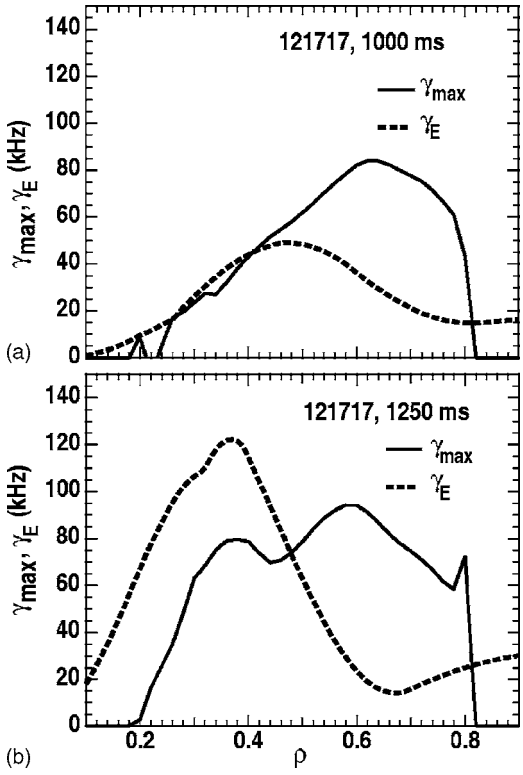

FIG. 14. Profiles of maximum growth rate γ_{max} and $E\times B$ shearing rate γ_E for the shot of Fig. 13 for (a) $t=1000$ ms, before the ion barrier formation and (b) $t=1250$ ms, after the ion barrier formation.

χ_e, as indicated in the ECE data, would not be expected to be visible in the TRANSP analysis due to the smoothing and time averaging involved.) This χ_e behavior is consistent with the lack of a sustained electron transport barrier. In general in DIII-D, electron ITBs are only seen in strongly reversed shear discharges, not moderate shear discharges like the ones discussed here.

The ion ITB formation in these shots follows the standard $E\times B$ shear picture, as indicated in Fig. 14. This figure shows the maximum growth rate calculated from GKS (Ref. 27) simulations, γ_{max}, and the corresponding experimental $E\times B$ shearing rate, γ_E for two times, one 150 ms before the $q_{min}=2$ time and the transition event, and one 100 ms after. The experimental shearing rate is calculated from the ion radial force balance equation using measurements of ion temperature and toroidal and poloidal rotation. At the earlier time γ_E is of the order of γ_{max} inside of $\rho=0.5$; at the later time, γ_E greatly exceeds γ_{max} in the core. A recent paper[28] shows that the ratio γ_E/γ_{max} needs to exceed 2 in order to quench ITG/TEM transport. In light of this, the discharge at 1000 ms is expected to be marginal for barrier formation, while at 1250 ms reduced transport is expected in the core, in agreement with the experiment. It should be noted here that the q profile plays no part in the determination of the maximum growth rate. It is the transient effect of the zonal flow structure at the rational q value that pushes the shearing rate above the value to initiate suppression of turbulence and the plasma bootstraps itself into improved confinement.

IV. SUMMARY AND CONCLUSIONS

In this paper we have shown that, in a specific class of DIII-D discharges, ion and electron transport change in the vicinity of integer q_{min}. In general the electron transport reduction is transient while the ion transport can be transient or an enduring core barrier can form depending on the total input power. These results are similar to those from other tokamaks,[3–8] and integer q surfaces are widely recognized as zones of improved confinement in plasma devices.

The DIII-D data show clearly that the confinement changes precede the q_{min}=integer time. This has implications for the triggering mechanism, one of which is that it precludes the presence of magnetic islands and their accompanying changes to E_r as a required/necessary condition. Magnetic islands might be playing a role in similar discharges in other tokamaks: as mentioned earlier, these low power NCS discharges are generally marginal for barrier formation, and any small perturbation that alters E_r could push the shearing rate above the threshold value for turbulence suppression and ensuing confinement improvement. But with the low β values in the discharges analyzed here, large MHD islands are not observed in the vicinity of integer q in the pre-ITB phase.

Significant changes to turbulent fluctuation levels have been observed near integer q_{min}. The BES data show localized reductions of low-k density fluctuations in the region of the q_{min} radius and these dips correlate in time with the improvement in electron transport at the same location. For the intermediate k fluctuations of the FIR scattering data it is seen that the turbulence level in the core drops at the $q_{min}=2$ time when the core barrier forms and the turbulence remains at a reduced level during the improved core confinement phase. This observation is consistent with the picture of core barrier formation via $E\times B$ shear suppression, where at the time of integer q the shear changes appreciably near the half radius and the growth rate for the dominant mode is exceeded, spurring the plasma into the improved confinement regime.

Finally, the T_e gradient measurements near the integer q_{min} time are in agreement with results from the GYRO code that predict the presence of profile corrugations tied to low order rational values of q. These zonal flow structures occur due to the gap in rational surfaces near integer q surfaces and explain the observed temperature changes just before and just after q_{min}=integer is crossed. The profile corrugations are seen to be larger for a low shear case where the spatial extent of the gap in q surfaces is wider. The experimental T_e gradient profile corrugations have only been seen to date in L-mode discharges, not in the H-mode. One implication of the GYRO result is that the corrugations, which are pumped by high-n turbulence, may be smaller in an H-mode plasma with its reduced level of turbulent fluctuations. More experiments are planned on DIII-D to verify the GYRO results and the effect of zonal flows near low order rational q surfaces.

The physics picture of the core barrier formation that emerges from the data and the GYRO calculations has several interlinked components. As q_{min} approaches an integer value, the zonal flow structure driven by the turbulence grows up to a significant amplitude because of the low den-

sity of rational surfaces. Because of low magnetic shear near $q_{\min}$, this zonal flow structure has a significant radial extent. The oscillating $E\times B$ shear associated with the zonal flows produces changes in local, turbulent-driven transport leading to the increase in local temperature gradients away from the $q=$integer point seen in the data. These zonal-flow-induced changes are transient effects, localized around the $q=$integer unless the equilibrium $E\times B$ shear associated with the background profiles is a certain magnitude. If the equilibrium $E\times B$ shear is large enough, i.e., close to the value needed to decorrelate the turbulence, then the zonal-flow-induced transient can trigger changes in the equilibrium profiles which lead to the formation of a sustained core transport barrier. Accordingly, the essential physics affecting the turbulent transport is $E\times B$ shearing, part of which is produced by the zonal flows and the rest by the background, equilibrium profiles. The key synthesis here is the realization that the zonal flows are sensitive to the magnetic field structure near integer q surfaces and their action provides the impetus that leads to the changes in turbulence and transport.

ACKNOWLEDGMENTS

This work was supported by the U.S. Department of Energy under Contract Nos. DE-FG03-97ER54415, DE-FC02-04ER54698, SC-G903402, DE-FG02-92ER54141, W-7405-ENG-48, DE-FG03-96ER54373, DE-FG03-01ER54615, and DE-AC05-76OR00033.

[1] J. L. Luxon and L. G. Davis, Fusion Technol. **8**, 441 (1985).
[2] C. M. Greenfield, C. L. Rettig, G. M. Staebler *et al.*, Nucl. Fusion **39**, 1723 (1999).
[3] Y. Koide, M. Kikuchi, M. Mori *et al.*, Phys. Rev. Lett. **72**, 3662 (1994).
[4] M. R. de Baar, M. N. A. Beurskens, G. M. D. Hogeweij, and N. J. Lopes Cardozo, Phys. Plasmas **6**, 4645 (1999).
[5] M. Bell, R. E. Bell, P. C. Efthimion *et al.*, Plasma Phys. Controlled Fusion **41**, A719 (1999).
[6] E. Joffrin, G. Gorini, C. D. Challis *et al.*, Plasma Phys. Controlled Fusion **44**, 1739 (2002).
[7] S. Günter, S. D. Pinches, G. D. Conway, A. Gude, J. Hobirk, M. Maraschek, A. G. Peeters, R. C. Wolf, and the ASDEX Upgrade Team, in Proceedings of the 28th European Physical Society Conference on Controlled Fusion and Plasma Physics, Funchal, 2001 (European Physical Society, 2001), Vol. 25A, p. 49.
[8] K. A. Razumova, A. A. Borschegovskii, V. V. Chistyakov *et al.*, in Proceedings of the 19th International Conerence on Fusion Energy, Lyon, 2002 (IAEA, Vienna, 2002), CD-ROM file IAEA-CN-94/EX/P3-03 and http://www.iaea.org/programmes/ripc/physics/fec2002/ html/fec2002.htm
[9] X. Garbet, C. Bourdelle, G. T. Hoang, P. Maget, S. Benkadda, P. Beyer, C. Figarella, I. Voitsekovitch, O. Agullo, and N. Bian, Phys. Plasmas **8**, 2793 (2001).
[10] J. H. Misguish, J-D. Reuss, D. Constantinescu, G. Steinbrecher, M. Vlad, F. Spineanu, B. Weyssow, and R. Balescu, Plasma Phys. Controlled Fusion **44**, L29 (2002).
[11] J. D. Callen, Phys. Rev. Lett. **94**, 055002 (2005).
[12] B. W. Rice, D. G. Nilson, K. H. Burrell, and L. L. Lao, Rev. Sci. Instrum. **70**, 815 (1999).
[13] S. E. Sharapov, B. Alper, H. L. Berk, and D. Borba, Phys. Plasmas **9**, 2027 (2002).
[14] R. Nazikian, G. J. Kramer, R. V. Budny *et al.*, in Proceedings of the 20th IAEA Fusion Energy Conference (Vilamoura, Portugal, 2004).
[15] C. L. Rettig, S. Burns, R. Philipona, W. A. Peebles, and N. C. Luhman, Jr., Rev. Sci. Instrum. **61**, 3010 (1990).
[16] E. Joffrin, C. D. Challis, G. D. Conway *et al.*, Nucl. Fusion **43**, 1167 (2003).
[17] J. Candy and R. E. Waltz, J. Comput. Phys. **186**, 545 (2003).
[18] R. E. Waltz, J. Candy, F. L. Hinton, C. Estrada-Mila, and J. E. Kinsey, Nucl. Fusion **45**, 741 (2005).
[19] P. H. Diamond, S.-I. Itoh, K. Itoh, and T. S. Hahm, Plasma Phys. Controlled Fusion **47**, R35 (2005).
[20] R. E. Waltz, M. E. Austin, K. H. Burrell, and J. Candy, Phys. Plasmas **13**, 052301 (2006).
[21] G. J. Kramer, R. Nazikian, B. Alper *et al.*, Phys. Plasmas **13**, 056104 (2006).
[22] W. W. Heidbrink, K. H. Burrell, Y. Luo, N. A. Pablant, and E. Ruskov, Plasma Phys. Controlled Fusion **46**, 1855 (2004).
[23] D. K. Gupta, R. J. Fonck, G. R. McKee, D. J. Schlossberg, M. W. Shafer *et al.*, Rev. Sci. Instrum. **75**, 3493 (2004).
[24] G. R. McKee, C. C. Petty, R. E. Waltz *et al.*, Nucl. Fusion **41**, 1235 (2001).
[25] K. H. Burrell, Phys. Plasmas **4**, 1499 (1997).
[26] C. M. Greenfield, J. C. DeBoo, T. C. Luce *et al.*, Phys. Plasmas **7**, 1959 (2000).
[27] M. Kotschenreuther, W. Dorland, M. A. Beer, and G. W. Hammett, Phys. Plasmas **2**, 2381 (1995).
[28] J. E. Kinsey, R. E. Waltz, and J. Candy, Phys. Plasmas **12**, 062302 (2005).